Stabilization of thermoacoustic oscillators by delay coupling

H. Hyodo* and T. Biwa
Department of Mechanical Engineering, Tohoku University, Sendai 980-8579, Japan

(Received 24 July 2018; published 26 November 2018)

This paper presents a numerical description of amplitude death in delay-coupled thermoacoustic oscillators. An oscillator is a gas-filled resonance tube with a temperature gradient. Delay coupling is introduced by hollow tubes that connect the oscillators. Thermoacoustic oscillators and their connecting tubes are modeled by linear acoustic equations. For them, two coupling methods are tested: single-tube and double-tube coupling. For single-tube coupling, amplitude death occurs when the connecting tube length is one-quarter or three-quarters of the wavelength of the oscillation frequency and when the tube diameter is greater than 62.5% of the resonance tube diameter. For double-tube coupling, amplitude death occurs with specific combinations of the tube lengths given by integer multiples of the half-wavelength. The required tube diameter is as small as 7.5% of the resonance tube diameter. Death regions for the double-tube coupling are verified from the experimentally obtained results. Comparison with the delay-coupled van der Pol oscillators highlights acoustic aspects of the double-tube coupling.

DOI: 10.1103/PhysRevE.98.052223

I. INTRODUCTION

Amplitude death refers to complete annihilation of self-sustained oscillations observed when two or more oscillators are mutually coupled [1–9]. Although dissipative coupling is unable to stop oscillations of the coupled identical oscillators with zero detuning, Reddy *et al.* demonstrated that time-delay coupling led to the amplitude death in the absence of detuning [10]. Amplitude death was studied theoretically for paradigmatic model oscillators [10,11], where islandlike death regions were found under specific combinations of delay time and coupling strength. More recently, various delay-coupling methods [12–15] were studied. For example, a coupling using multiple delay times has been shown to suppress oscillations of the coupled oscillators even with an extremely long delay time [16]. Because finite propagation speeds of signals are ubiquitous in nature, delay-induced amplitude death is expected to occur in various real systems, as well as those reported in coupled laser systems [17], electronic circuits [18], and chemical reaction systems [7].

This study explores the amplitude death regions that exist when two thermoacoustic oscillators are coupled with a time delay. A thermoacoustic oscillator is made of a gas-filled resonance tube that has a local temperature gradient. The gas in the resonance tube begins to oscillate spontaneously when the temperature gradient becomes sufficiently large. The resulting intense acoustic oscillations are often dangerous and harmful. For example, Taconis oscillation [19], i.e., thermoacoustic oscillations in a narrow tube that is put into a liquid-helium vessel from outside, causes rapid evaporation of liquid helium. Combustion oscillations [20,21] in gas turbine engine combustors are also unwanted thermoacoustic oscillations because they can engender severe damage to the engine structure. Development of a simple and reliable suppression method is an urgent necessity for the further development of combustion systems, such as those using a lean premixed combustion reaction.

Recently, the amplitude death phenomenon was explored experimentally in thermoacoustic oscillators that were coupled with delay and diffusive couplings [6]. Delay coupling was introduced simply by a hollow tube connecting the two resonance tubes. The delay time was controlled through the tube length because the propagation time for the acoustic wave to pass through the tube gives the delay time. The experimental death regions on the plane of the coupling strength versus the delay time were compared with delay-coupled van der Pol systems. Although qualitative agreement was achieved between them, the coupling term for the coupled van der Pol systems was assumed using the difference between the signal of one oscillator and the delayed signal of the other, without consideration of the acoustic properties of the gas column in the connecting tube. Using a numerical approach, amplitude death in coupled thermoacoustic oscillators was studied by Thomas *et al.* [22]. After they derived a model equation of a Rijke tube thermoacoustic oscillator based on the acoustic basic equation, they discussed the result of time-delay and dissipative couplings to elucidate the possibility of amplitude death. The coupling terms are, however, expressed by the difference between acoustic variables without stating how such couplings are realized in real acoustic systems.

For full acoustic modeling of the coupled thermoacoustic oscillator, we adopt linear acoustic theory [23,24], which has been established in a study of marginal conditions of thermoacoustic oscillations [25–29]. Two thermoacoustic oscillators and connecting tubes are modeled using linearized hydrodynamic equations. The tube length and diameter are chosen as calculation parameters. The resulting death regions are compared with the experimentally obtained results. This paper describes the finding that coupling by the two tubes, each having a different length, can achieve amplitude death with a smaller radius than the single-tube coupling. The

*hyodo@amsd.mech.tohoku.ac.jp

present result is compared with those obtained for coupled van der Pol oscillators to demonstrate the importance of acoustic modeling of the connecting tube.

II. PHYSICAL MODEL FOR COUPLED THERMOACOUSTIC OSCILLATORS

A. Thermoacoustic oscillator

A thermoacoustic oscillator employed in this study is presented in Fig. 1(a). This type of oscillator, which is made of a resonance tube installed with a stack and adjacent heat exchangers, is known as a standing-wave thermoacoustic oscillator [30]. For this study, a circular tube of diameter $D = 40$ mm and length $L = 860$ mm is used as a resonance tube. The tube, with both ends closed, contains 1-bar air as the working gas. The stack is located in the resonance tube with its central position separated from the end by 180 mm. The stack is assumed to have many circular pores of 1.12 mm diameter and 40 mm length; the stack porosity is 0.78. Also, the stack is sandwiched between hot and cold heat exchangers, each of which is made of parallel plates with 0.5 mm thickness and 20 mm length, placed with 1 mm spacing. The temporal mean gas temperature, T_C, in the cold heat exchanger is constant at room temperature (297 K), whereas T_H in the hot heat exchanger is varied as a control parameter to induce thermoacoustic oscillation. The temporal mean gas temperature is changed linearly from T_C to T_H in the stack and also in the thermal buffer tube: an empty tube with 40 mm diameter and 30 mm length. In other parts of the oscillator, the temporal mean temperature is equal to T_C.

B. Coupled oscillators

Figure 1(b) presents a schematic representation of the coupled thermoacoustic oscillators. The oscillators are exact copies of each other. When uncoupled, they are as presented in Fig. 1(a). Coupling tubes, Tube A and Tube B, connect the oscillators at their ends at $x_1 = L$ and $x_2 = L$. Each tube has a circular channel with uniform diameter d and with length L_A or L_B. The effects of the tube curvature and the rapid change of the cross-sectional area at the tubes' connecting points are not considered. Tube length $L_{A,B}$ is related to the delay time by $L_{A,B}/c$, where c represents the speed of sound of the working gas. Tube radius d is related to the coupling strength.

We test two coupling methods: one is a single-tube coupling where the oscillators are coupled using Tube A; the other is a double-tube coupling using Tube A and Tube B simultaneously. For the single-tube coupling, stability analysis is performed with changing d and L_A. For the double-tube coupling, the stability is studied by changing L_A and L_B with a fixed value of d.

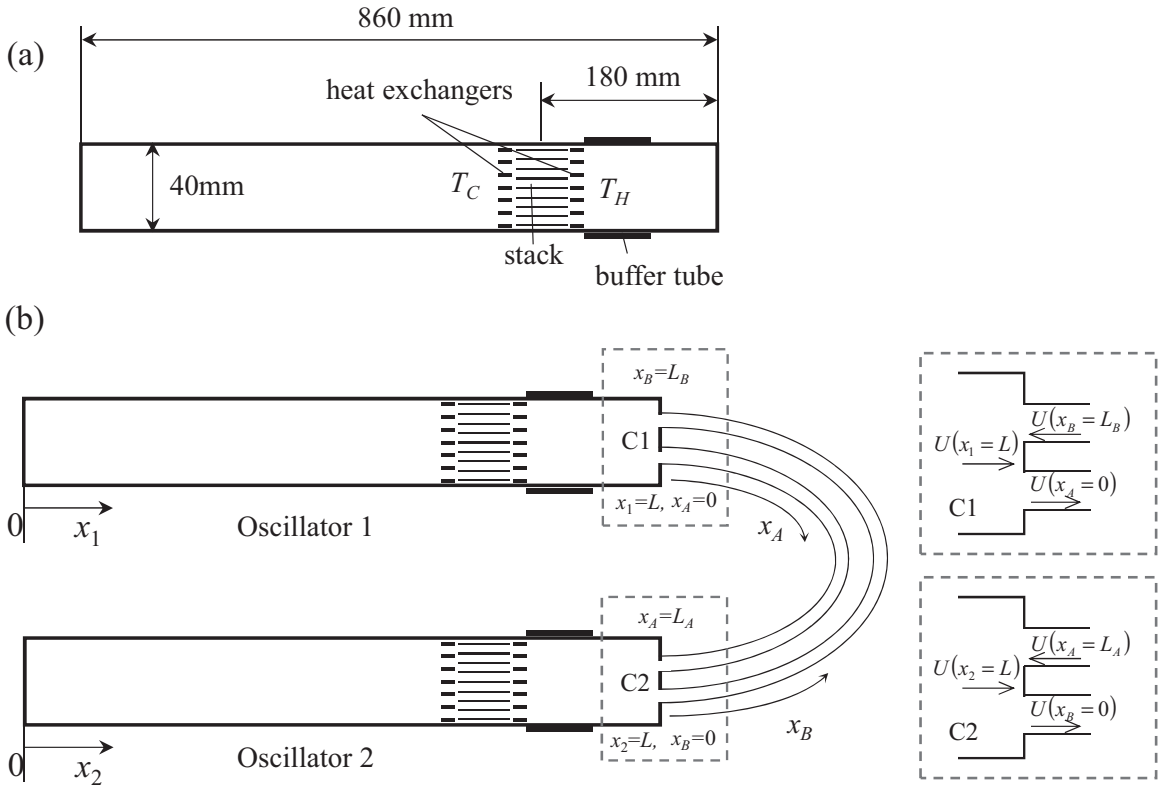

FIG. 1. Model thermoacoustic oscillator (a) and coupled oscillators (b). The axial coordinates $x_{1,2}$ are directed from cold to hot in the oscillator, with $x_{1,2} = 0$ at the end, where subscripts 1 and 2, respectively, correspond to Oscillator 1 and Oscillator 2. The axial coordinates x_A and x_B along the connecting tubes, respectively, start from Oscillator 1 and end at Oscillator 2 and start from Oscillator 2 and end at Oscillator 1, where A and B, respectively, stand for Tube A and Tube B. Close up views of junctions C1 and C2 between the oscillators and the connecting tubes are also shown in the dashed squares.

III. CALCULATION METHOD

A. Basic equations

In this calculation, the hydrodynamic equations of continuity, momentum, and energy are used to describe the longitudinal acoustic gas oscillations. The state equation of an ideal gas is used as well. Acoustic variables φ are expressed as a sum of the temporal mean value φ_m and the small disturbance φ' as $\varphi = \varphi_m + \varphi'$. The disturbances φ' are assumed to oscillate with angular frequency ω as $\varphi' = \Phi e^{i\omega t}$. Using Rott's acoustic approximation [23,30], the hydrodynamic equations are simplified to ordinary differential equations with respect to axial coordinate x. For the complex amplitude P of pressure and the complex amplitude U of volume velocity, they are given as

$$\frac{dP}{dx} = -ZU, \tag{1}$$

$$\frac{dU}{dx} = -YP + GU. \tag{2}$$

In Eqs. (1) and (2), Z, Y, and G are given as

$$Z = i\omega\frac{\rho_m}{A}\frac{1}{1-\chi_\nu}, \tag{3}$$

$$Y = i\omega\frac{A[1+(\gamma-1)\chi_\alpha]}{\gamma P_m}, \tag{4}$$

$$G = \frac{\chi_\alpha - \chi_\nu}{(1-\chi_\nu)(1-\sigma)}\frac{1}{T_m}\frac{dT_m}{dx}, \tag{5}$$

where ρ_m, P_m, and T_m, respectively, denote the temporal mean density, pressure, and temperature. Additionally, γ and σ are the specific-heat ratio and Prandtl number of the gas. For the gas with thermal diffusivity α and kinematic viscosity ν, the thermoacoustic function χ_j $(j = \alpha, \nu)$ is given using the first-order and zeroth-order Bessel functions J_1 and J_0 of the first kind as

$$\chi_j = \frac{2J_1[(i-1)\sqrt{\omega\tau_j}]}{(i-1)\sqrt{\omega\tau_j}J_0[(i-1)\sqrt{\omega\tau_j}]} \tag{6}$$

for a circular cylinder, whereas it is given as

$$\chi_j = \frac{\tanh[(1+i)\sqrt{\omega\tau_j}]}{(1+i)\sqrt{\omega\tau_j}} \tag{7}$$

for parallel plates. In both equations, τ_j $(j = \alpha, \nu)$ is written as

$$\tau_j = r^2/(2j), \tag{8}$$

where r denotes the radius in the case of the circular cylinder and the half of the plate distance in the case of parallel plates.

In a flow channel with a uniform cross section, the differential equations are solved analytically if coefficients Z, Y, and G are regarded as constants. When pressure $P(x)$ and volume velocity $U(x)$ at a point x are given, the solution gives $P(x+l)$ and $U(x+l)$ at a point $x+l$ as

$$\begin{bmatrix} P(x+l) \\ U(x+l) \end{bmatrix} = M\begin{bmatrix} P(x) \\ U(x) \end{bmatrix}, \tag{9}$$

where M is the transfer matrix expressed as

$$M = e^{\frac{Gl}{2}}\begin{bmatrix} -\frac{G}{b}\sinh\lambda + \cosh\lambda & -\frac{2Z}{b}\sinh\lambda \\ -\frac{2Y}{b}\sinh\lambda & \frac{G}{b}\sinh\lambda + \cosh\lambda \end{bmatrix}, \tag{10}$$

with $b = \sqrt{G^2 + 4YZ}$ and $\lambda = bl/2$.

For the flow channel with nonzero dT_m/dx, such as the regenerator and the thermal buffer tube, we divide it into short segments where temperature-dependent gas properties can be assumed as constants. The transfer matrices of the regenerator and the thermal buffer tube are constructed by assuming a linear temperature distribution with end temperatures T_C and T_H, and subsequently by calculating a product of the transfer matrices of equally divided segments, where the gas thermal properties are estimated from the spatial average of T_m. The division number is 10. We confirmed that the results were almost unchanged when it was increased to 100.

For flow channels with uniform temperature, the transfer matrices are determined by specifying the flow channel type and size and by setting $G = 0$ in Eq. (10). This case applies to hot and cold heat exchangers, and to circular tubes with diameter D.

The combined transfer matrix M_E of the thermoacoustic oscillator is created using a product of the transfer matrices of the circular tube, cold heat exchanger, regenerator, hot heat exchanger, thermal buffer tube, and the circular tube. Transfer matrices M_A and M_B of the connecting tubes are created in the same way as the uniform temperature flow channel by ignoring tube curvature effects.

B. Derivation of the frequency equation

Transfer matrix M_E links acoustic variables $(P_{1,2}(0), U_{1,2}(0))$ at $x_{1,2} = 0$ with $(P_{1,2}(L), U_{1,2}(L))$ at $x_{1,2} = L$ on both ends of the oscillator:

$$\begin{bmatrix} P_{1,2}(L) \\ U_{1,2}(L) \end{bmatrix} = M_E\begin{bmatrix} P_{1,2}(0) \\ U_{1,2}(0) \end{bmatrix}. \tag{11}$$

Transfer matrix $M_{A,B}$ links acoustic variables $(P_{A,B}(0), U_{A,B}(0))$ with $(P_{A,B}(L_{A,B}), U_{A,B}(L_{A,B}))$ at the ends of the connecting tube, as shown below,

$$\begin{bmatrix} P_{A,B}(L_{A,B}) \\ U_{A,B}(L_{A,B}) \end{bmatrix} = M_{A,B}\begin{bmatrix} P_{A,B}(0) \\ U_{A,B}(0) \end{bmatrix}. \tag{12}$$

At the closed ends of the uncoupled oscillators $(x_{1,2} = 0, L)$, the boundary conditions require $U_{1,2} = 0$. To have a nonzero solution,

$$(M_E)_{21} = 0 \tag{13}$$

must hold. This equation serves as the frequency equation of the uncoupled oscillator, where the two subscript numbers denote the transfer-matrix component.

The connecting conditions between the oscillator and the connecting tube are the continuity of pressure,

$$P_1(L) = P_A(0), \quad P_2(L) = P_A(L), \tag{14}$$

and the continuity of the volume velocity. The latter is expressed for the single-tube coupling as

$$U_1(L) = U_A(0), \quad U_2(L) = -U_A(L) \tag{15}$$

and for the double-tube coupling as

$$U_{1,2}(L) + U_{B,A}(L_{B,A}) = U_{A,B}(0). \tag{16}$$

As a condition to have a nonzero solution of P and U, we obtain the frequency equation as

$$(M_A)_{21}(M_E)_{11}^2 + [(M_A)_{11} + (M_A)_{22}](M_E)_{11}(M_E)_{21} + (M_A)_{12}(M_E)_{21}^2 = 0 \tag{17}$$

for the coupled oscillators with a single connecting tube, and

$$\begin{aligned} &H_1 H_2 - H_3 H_4 = 0, \\ &H_1 = \left(\frac{(M_E)_{21}}{(M_E)_{11}} + \frac{(M_A)_{11}}{(M_A)_{12}} + \frac{(M_B)_{22}}{(M_B)_{12}}\right), \\ &H_2 = \left(\frac{(M_E)_{21}}{(M_E)_{11}} + \frac{(M_B)_{11}}{(M_B)_{12}} + \frac{(M_A)_{22}}{(M_A)_{12}}\right), \\ &H_3 = \left((M_A)_{21} - \frac{(M_A)_{11}(M_A)_{22}}{(M_A)_{12}} - \frac{1}{(M_B)_{12}}\right), \\ &H_4 = \left((M_B)_{21} - \frac{(M_B)_{11}(M_B)_{22}}{(M_B)_{12}} - \frac{1}{(M_A)_{12}}\right) \end{aligned} \tag{18}$$

for the coupled oscillators with two connecting tubes.

C. Calculation procedure

When T_H is given for the uncoupled oscillator, Eqs. (13), (17), and (18) can be regarded as applicable equations with respect to $f = \omega/(2\pi)$. Solution f is generally a complex quantity [26,28,31]. The real part f_R represents the frequency of the fluctuation. The imaginary part f_I reflects the stability of the equilibrium state with $P = 0$ and $U = 0$; a positive imaginary part means that the equilibrium state is linearly stable, whereas a negative one indicates that the equilibrium state is unstable. When solution f becomes a real number, the equilibrium state is neutrally stable.

Figure 2 presents complex frequency $f = f_R + if_I$ as a function of temperature difference $\Delta T = T_H - T_C$ in the uncoupled thermoacoustic oscillator. It was obtained numerically from Eq. (13) using the Newton method for the fundamental and second-mode oscillations. When ΔT is increased, f_R of the fundamental mode remains at around 200 Hz, whereas that of the second mode is around 400 Hz. These frequencies closely approximate $L/(2c)$ and L/c. The imaginary part f_I of the fundamental mode decreases and becomes negative with $\Delta T > 190$ K, whereas f_I of the second mode remains positive even when $\Delta T = 250$ K. This result means that only the fundamental mode is generated in the uncoupled oscillator in the region $190 < \Delta T < 250$ K. In the following, ΔT is set to 240 K to investigate whether the oscillations are suppressed by delay coupling.

For the coupled thermoacoustic oscillators, Eqs. (17) and (18) can also be regarded as equations with respect to f when T_H, d, L_A, and L_B are given. The solutions f are calculated by changing the coupling tube parameters. The phase difference ϕ between Oscillator 1 and Oscillator 2 is calculable by inserting solution f into M_A in Eq. (12) and then by ascertaining the phase relation between $P_A(L_A)$ and $P_A(0)$.

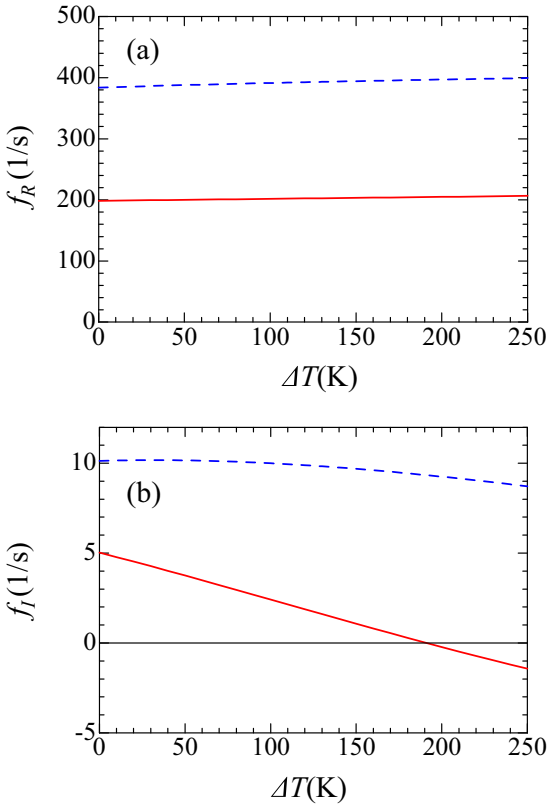

FIG. 2. Real part f_R (a) and imaginary part f_I (b) of the uncoupled thermoacoustic oscillator. The solid curve corresponds to the fundamental mode oscillations of the resonance tube, whereas the broken curve represents second-mode oscillations.

IV. CALCULATION RESULTS

A. Single-tube coupling

Figure 3 portrays the tube length dependence of f_R and f_I for the single-tube coupling obtained by finding the solution $f = f_R + if_I$ of Eq. (17). The tube diameter is fixed at 30 mm. The three continuous curves I_1, A, and I_2 are presented to distinguish the oscillation modes. For modes I_1 (solid curve) and I_2 (broken curve), the phase difference ϕ between the pressure $P_1(L)$ and $P_2(L)$ becomes 0 (in-phase oscillations), whereas ϕ becomes 180° (antiphase oscillation) for mode A (dotted curve). For the connecting tube, we have confirmed a pressure maximum in the middle of the tube for I_1, two pressure maxima for I_2, and a pressure minimum for A. The equilibrium state of the coupled oscillators remains stable if f_I is positive for all of these oscillation modes. Results show that coupling-induced amplitude death occurs in regions with $0.35 \leqslant L_A \leqslant 0.5$ m, $1.16 \leqslant L_A \leqslant 1.39$ m, and $L_A \geqslant 1.9$ m. In other regions of L_A, at least one oscillation mode should be excited because the smallest values of f_I become negative. In other words, the stability of the equilibrium state of the coupled oscillators can be judged by investigating the smallest f_I values among these oscillation modes.

Figure 4 presents a contour map of f_I on the plane of L_A and d. Broken curves represent the contour line with $f_I = 0$. In the upper part of the broken curves, f_I is positive. Therefore, amplitude death occurs in these areas. The smallest

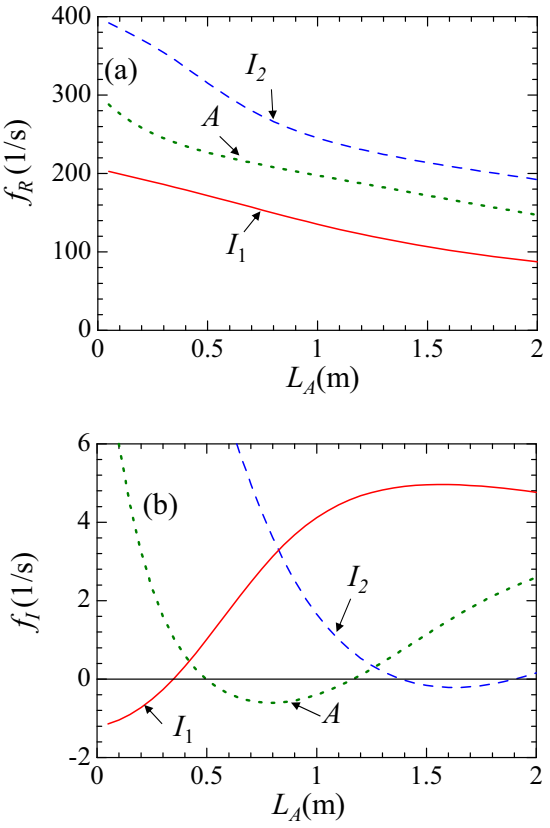

FIG. 3. Real component f_R (a) and imaginary component f_I (b) for $0.05 \leqslant L_A \leqslant 2.0$ m with $d = 30$ mm. Labels represent the oscillation mode between Oscillator 1 and Oscillator 2: I_1 (solid curve) and I_2 (broken curve) represent in-phase oscillations, whereas A (dotted curve) shows antiphase oscillations.

value of d in the amplitude death regions is $d = 25$ mm at $L_A = 1.26$ m. When $d = 40$ mm, the amplitude death region extends to $0.22 \leqslant L_A \leqslant 0.62$ m, to $1.1 \leqslant L_A \leqslant 1.6$ m, and to $L_A \geqslant 1.7$ m. The center values of L_A are close to one-quarter

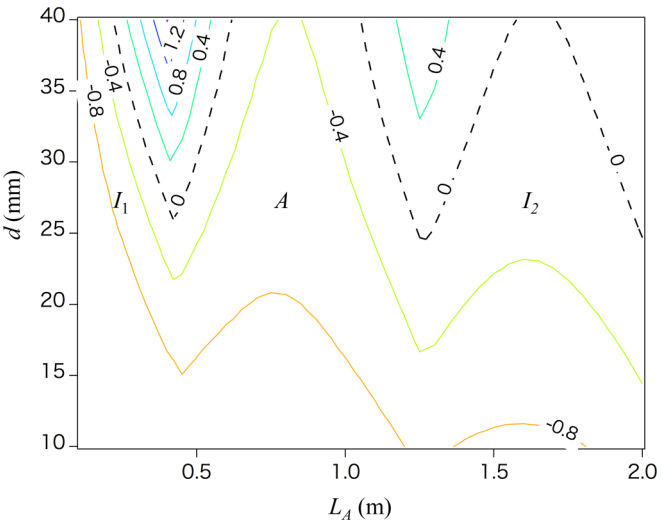

FIG. 4. Contour map of the imaginary part f_I on L_A vs d. The meanings of labels $I_{1,2}$ and A in Fig. 4 are the same as those in Fig. 3.

or three-quarters of the wavelength of 205 Hz fundamental acoustic waves. Delay time τ is given by $\tau = L_A/c$. Therefore, amplitude death occurs with $\tau = T/4$ and $3T/4$, where T is an acoustic period of the fundamental mode. This result is consistent with the theory and experiments for other systems [11,18].

Phase difference ϕ was calculated using the solution f having the smallest f_I value. On the left side of $L_A = 0.42$ m, mode I_1 with $\phi = 0$ is excited. In the region with $0.42 < L_A < 1.27$ m, mode A with $\phi = 180^\circ$ has the lowest value of f_I. On the right side of $L_A = 1.27$ m, the phase difference becomes $\phi = 0$ again, but in this region, mode I_2 is excited instead of I_1. Results show that the amplitude death occurs at the boundary between the in-phase and antiphase oscillation mode. This result is consistent with Reddy's experiments with electrical circuits [18].

B. Double-tube coupling

Linear stability of the coupled thermoacoustic oscillators with two tubes is obtained by finding the solution f of Eq. (18). Figure 5 shows the contour map of f_I on the plane of L_A and L_B when tube diameter d is 8 mm in Tube A and Tube B. Although the tube diameter must be as high as 25 mm in the case of single-tube coupling, death regions are created with $d = 8$ mm for double-tube coupling. The difference of the required tube diameter is discussed later. Contour lines are extremely dense inside the death regions. The peak value of f_I on the center of the islands is 2.12 (1/s). Therefore, the

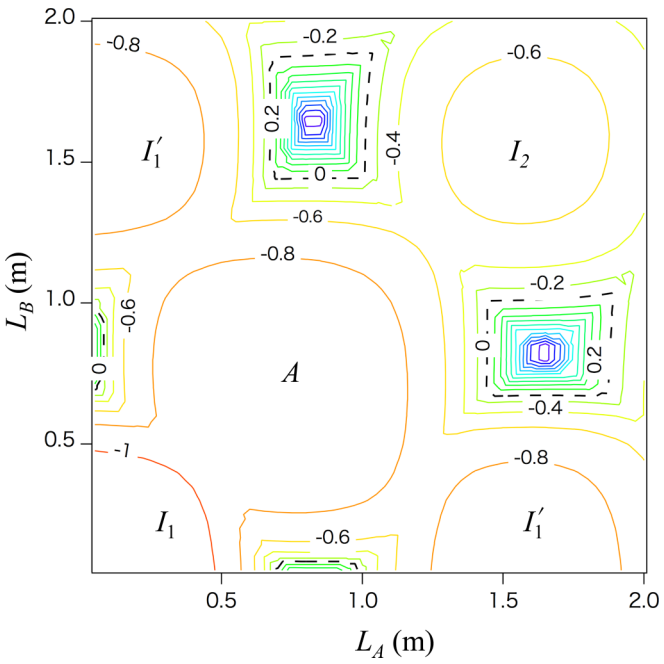

FIG. 5. Contour map of the imaginary part of $f(=\omega/2\pi)$ on L_A vs L_B for $d = 8$ mm. Labels I_1, I_1', and I_2 represent the in-phase oscillation mode. I_1' means that the shorter connecting tube has a pressure maximum, and that the longer one contains two pressure maxima. I_1 and I_2, respectively, denote that two connecting tubes contain one pressure maximum and two pressure maxima. Mode A is the antiphase oscillation mode.

oscillations will cease shortly after $1/(2\pi f_I) = 1/13$ s when the coupling is switched on.

The death islands are centered at positions with $(L_{A,B}, L_{B,A}) = (0.85\ \text{m},\ 0.05\ \text{m})$ and $(L_{A,B}, L_{B,A}) = (1.7\ \text{m}, 0.85\ \text{m})$. Two lengths $L_{A,B} = 0.85$ and 1.7 m, respectively, correspond to $\tau = T/2$ and $\tau = T$ of the 205 Hz acoustic wave. Amplitude death occurred with $L_A = 0.42$ and 1.27 m in the case of the single-tube coupling most easily, but the combinations of $(L_A, L_B) = (0.42\ \text{m},\ 0.42\ \text{m})$, (1.27 m, 1.27 m), and $(L_{A,B}, L_{B,A}) = (0.42\ \text{m},\ 1.27\ \text{m})$ fail to stop the oscillations in the case of double-tube coupling. It is noteworthy that the tube length realizing amplitude death differs between single-tube coupling and double-tube coupling. The amplitude death brought about by the combinations of specific tube lengths is a distinctive property of the double-tube coupling in the thermoacoustic oscillators, as we demonstrate later through comparison with the coupled van der Pol oscillators.

The phase difference ϕ between the oscillators was calculated for the case of double-tube coupling. Modes I_1, I_1', and I_2 represent the in-phase oscillation mode, which appears when the oscillators are coupled by two tubes with the length that makes in-phase oscillation for single-tube coupling. In modes I_1 and I_2, two connecting tubes, respectively, contain one pressure maximum and two pressure maxima. In mode I_1', the shorter connecting tube contains a pressure maximum. The longer one contains two pressure maxima. Mode A is the antiphase oscillation mode. The system becomes the antiphase oscillation mode when the oscillators are coupled by two tubes with the length that makes the antiphase oscillation mode for single-tube coupling.

As described above, the tube diameter necessary for amplitude death was $d = 8$ mm diameter in double-tube coupling, although it was $d = 25$ mm in single-tube coupling. Here we discuss the d dependence of f_I to see minimum d leading to amplitude death. Contour maps such as that of Fig. 5 were further created for d values less than 8 mm. The peaks of f_I were persistently centered near the points $(L_{A,B}, L_{B,A}) = (0.85, 1.7)$, but their height changed as shown in Fig. 6. The largest value $f_{I\max}$ increased to $f_{I\max} = 4.61$ (1/s) at $d = 4.5$ mm; then it started to decrease and cross zero between $d = 3$ and 2 mm. This result indicates that the double-tube coupling can achieve amplitude death with $d = 3$ mm that is as small as 7.5% of the oscillator diameter. This is a great reduction of the tube diameter because $d = 25$ mm, which is 62.5% of the oscillator diameter, was necessary in the single-tube coupling. Therefore, the double-tube coupling is a powerful means of achieving amplitude death in the thermoacoustic system. We also observed that the size of the death islands became small monotonically with decreasing d. An accurate choice of the coupling tube lengths is necessary to stop oscillations with small d. Future work is necessary to find ways of further increasing the peak value of $f_{I\max}$.

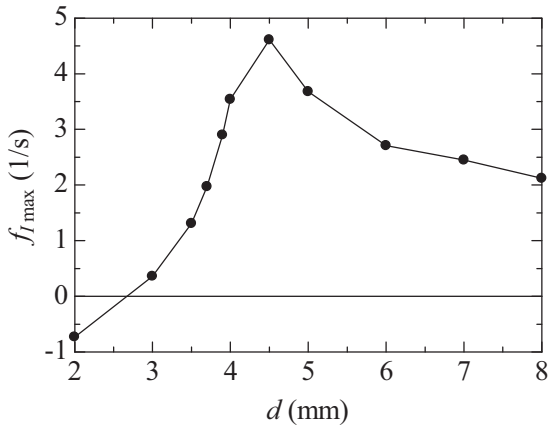

FIG. 6. Tube diameter dependence of $f_{I\max}$, which is the largest value on the contour map for each d.

C. Comparison with experiment

To verify the calculation results of double-tube coupling, we tested it through experimentation. A stainless-steel circular tube was used to construct the resonance tube of the oscillator in Fig. 1(a). The regenerator was made with a ceramic honeycomb catalyst support having square pores with sides of 1.12 mm. The hot heat exchanger temperature T_H was controlled by feeding an electrical current to a heater wire wound around it. The cold heat exchanger was kept at room temperature T_C by circulating water around the tube. When the temperature difference $\Delta T = T_H - T_C$ reached a critical value, it was confirmed that the gas column in the resonance tube began to oscillate spontaneously with the fundamental mode. After this observation, we prepared the other set of components to build the second oscillator. The two oscillators were connected by thick-walled flexible tubes mounted on the closed end. The tube diameter was 8 mm. Pressure oscillations were monitored using pressure transducers located at the closed end of each oscillator. The temperature difference was kept at $\Delta T = 280$ K, which led to a pressure amplitude of 3.1 kPa and an oscillation frequency of $f = 215$ Hz in the uncoupled thermoacoustic oscillator.

Figure 7 presents the contour map of pressure amplitude P_1 on the plane of L_A and L_B when the two oscillators were coupled by the two tubes. The color shows the magnitude of the pressure amplitude. The pressure amplitude P_2 was almost identical to P_1. The amplitude became zero near at the point of $(L_{A,B}, L_{B,A}) = (0.8\ \text{m},\ 1.6\ \text{m})$, as presented in Fig. 7. Near $(L_{A,B}, L_{B,A}) = (0.8\ \text{m},\ 0.0\ \text{m})$, the pressure amplitude did not become completely zero, but it was suppressed significantly below 0.2 kPa. Results show that the larger the imaginary part of the frequency in the calculation becomes, the smaller is the pressure amplitude in the experiment. We observed in-phase and antiphase synchronization outside of the amplitude death regions. The phase difference agreed with the calculation results. Results demonstrate that the stability analysis is useful for examining the amplitude death conditions in a thermoacoustic system.

V. DISCUSSION

As described in this section, amplitude death of the coupled thermoacoustic oscillators is compared with that of coupled van der Pol oscillators to assess the effects of acoustic wave propagation in the connecting tube upon amplitude death.

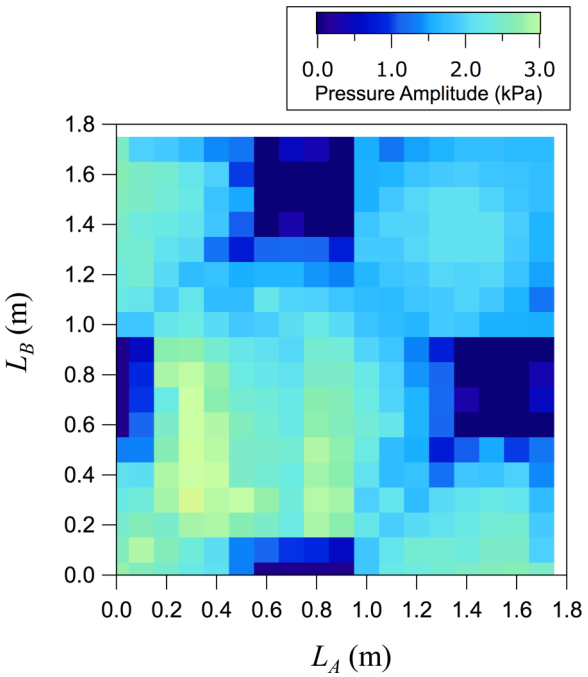

FIG. 7. Contour map of the pressure amplitude of oscillator 1 on L_A vs L_B for $d = 8$ mm.

The delay-coupled van der Pol oscillators are given as follows:

$$\ddot{x}_1 + (x_1^2 - \mu)\dot{x}_1 + \omega^2 x_1 = k_1[\dot{x}_2(t-\tau_1) - \dot{x}_1] + k_2[\dot{x}_2(t-\tau_2) - \dot{x}_1], \quad (19)$$

$$\ddot{x}_2 + (x_2^2 - \mu)\dot{x}_2 + \omega^2 x_2 = k_1[\dot{x}_1(t-\tau_1) - \dot{x}_2] + k_2[\dot{x}_1(t-\tau_2) - \dot{x}_2]. \quad (20)$$

In those expressions, μ, $k_{1,2}$, and $\tau_{1,2}$, respectively, represent coefficients of nonlinear damping, coupling strength, and delay time; also, ω denotes the intrinsic angular frequency. To reveal the linear stability around $x_1 = x_2 = 0$ and $\dot{x}_1 = \dot{x}_2 = 0$, Eqs. (19) and (20) are linearized. By assuming that the linear perturbation is given in the form of $e^{i\Omega t}$, the frequency equation is obtained as

$$[\omega^2 - \Omega^2 + i(k_1 + k_2 - \mu)\Omega]^2 + \Omega^2(k_1 e^{-i\Omega\tau_1} + k_2 e^{-i\Omega\tau_2})^2 = 0. \quad (21)$$

Using the Newton method, Eq. (21) is solved numerically in terms of $\Omega = \Omega_R + i\Omega_I$. The imaginary part Ω_I represents the linear stability [32]. In delay-coupled van der Pol oscillators, two oscillation modes are possible: in-phase synchronization oscillation mode I and antiphase synchronization oscillation mode A. Similarly to the explanation given in Sec. III, the solutions with the smallest Ω_I are chosen to judge the occurrence of amplitude death and the oscillation mode.

For comparison with single-tube coupling in a thermoacoustic system, Eq. (21) was solved for $k_2 = 0$. We set ω and μ as $\omega = 1.0$ and $\mu = 0.02$. Figure 8(a) presents the contour map of Ω_I shown on the plane of k_1 and τ_1. Broken curves represent the boundary on which $\Omega_I = 0$. On the upper side of the broken curves, Ω_I becomes positive. Therefore, these V-shaped regions are the amplitude death regions. The smallest k_1 able to cause amplitude death is $k_1 = 0.02$, which is equal to μ. Amplitude death regions appear when $\tau_1 = T/4$ and $3T/4$ ($T = 2\pi/\omega$), as in the coupled thermoacoustic system depicted in Fig. 4.

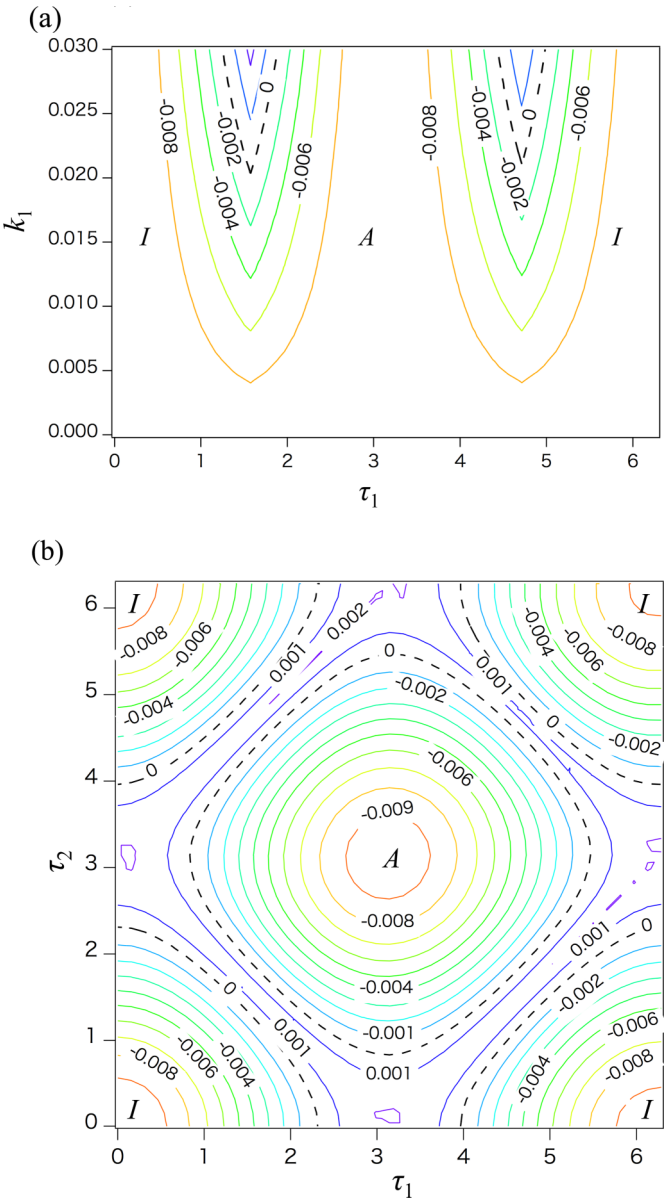

FIG. 8. Contour map of Ω_I in delay-coupled van der Pol oscillators: part (a) shows single delay-time coupling. The values of Ω_I are shown on the plane of k_1 vs τ_1; also, part (b) shows double delay-time coupling. The values of Ω_I are shown on the plane of τ_2 vs τ_1.

For comparison with double-tube coupling in a thermoacoustic system, Eq. (21) was solved for $k_1 = k_2 = k$, $\omega = 1.0$, and $\mu = 0.02$. For two time-delay coupling, the smallest k needed to cause the amplitude death was found to be $k = 0.01$: half of μ. Recalling that the necessary tube diameter was strongly reduced in the double-tube coupling, the two time-delay coupling results only in a moderate enhancement of stability of the equilibrium state. In other words, this

result indicates that the coupling terms in Eqs. (19) and (20) are insufficient to mimic the actual tube coupling of the thermoacoustic system. To map out the death region, k is chosen as $k = 0.012$ so that the amplitude death regions do not become too small. Figure 8(b) presents the contour map of Ω_I shown on the plane of τ_1 and τ_2. The amplitude death regions constitute diagonal lines in the van der Pol oscillators, whereas islandlike amplitude death regions were found in the thermoacoustic system, as presented in Fig. 5. In Fig. 8(b), the contour lines inside the amplitude death regions are less dense than in the region with $f_I < 0$. In Fig. 5, the contour lines in the regions with positive f_I are extremely dense compared to the other regions with negative f_I.

Therefore, differences exist, especially for double-tube coupling, in the amplitude death region and stability between the thermoacoustic oscillators modeled by the hydrodynamic equations and the van der Pol oscillators. Acoustic modeling of the coupling is expected to be necessary for a more realistic analysis of delay-induced amplitude death in combustion systems.

VI. SUMMARY

Stability analysis of the delay-coupled thermoacoustic oscillators was conducted based on the hydrodynamic equations. For single-tube coupling, amplitude death occurs when the connecting tube length is one-quarter or three-quarters of the wavelength of the oscillation frequency. For double-tube coupling, amplitude death occurs when the combined connecting tubes are a half-wavelength and one wavelength of the oscillation frequency. Comparison with the experimentally obtained results demonstrates that stability analysis based on the hydrodynamic equations can reproduce the location of experimentally observed amplitude death regions in coupled thermoacoustic oscillators, which differ from the death regions of delay-coupled van der Pol oscillators.

ACKNOWLEDGMENTS

This study was financially supported by JSPS KAKENHI Grants No. 15K17965 and No. 17K19064. The authors would like to thank I. Shinkai for his contribution to the experiments.

[1] K. Bar-eli, Physica D **14**, 242 (1985).
[2] R. Herrero, M. Figueras, J. Rius, F. Pi, and G. Orriols, Phys. Rev. Lett. **84**, 5312 (2000).
[3] Y. Zhai, I. Z. Kiss, and J. L. Hudson, Phys. Rev. E **69**, 026208 (2004).
[4] K. Suresh, M. D. Shrimali, A. Prasad, and K. Thamilamaran, Phys. Lett. A **378**, 2845 (2014).
[5] T. Banerjee and D. Ghosh, Phys. Rev. E **89**, 062902 (2014).
[6] T. Biwa, S. Tozuka, and T. Yazaki, Phys. Rev. Appl. **3**, 034006 (2015).
[7] R. Nagao, W. Zou, J. Kurths, and I. Z. Kiss, Chaos **26**, 094808 (2016).
[8] S. H. Strogatz, Nature (London) **394**, 317 (1998).
[9] G. Saxena, A. Prasad, and R. Ramaswamy, Phys. Rep. **521**, 205 (2012).
[10] D. V. Ramana Reddy, A. Sen, and G. L. Johnston, Phys. Rev. Lett. **80**, 5109 (1998).
[11] D. V. Ramana Reddy, A. Sen, and G. L. Johnston, Physica D **129**, 15 (1999).
[12] F. M. Atay, Phys. Rev. Lett. **91**, 094101 (2003).
[13] W. Zou and M. Zhan, Phys Rev E **80**, 065204 (2009).
[14] G. Saxena, A. Prasad, and R. Ramaswamy, Phys. Rev. E **82**, 017201 (2010).
[15] K. Konishi, H. Kokame, and N. Hara, Phys. Lett. A **374**, 733 (2010).
[16] K. Konishi, H. Kokame, and N. Hara, Phys. Rev. E **81**, 016201 (2010).
[17] P. Kumar, A. Prasad, and R. Ghosh, J. Phys. B **41**, 135402 (2008).
[18] D. V. Ramana Reddy, A. Sen, and G. L. Johnston, Phys. Rev. Lett. **85**, 3381 (2000).
[19] J. R. Clement and J. Gaffney, *Advances in Cryogenic Engineering*, Vol. 1 (Springer, Boston, MA, 1960).
[20] T. C. Lieuwen and V. Yang, *Combustion Instabilities in Gas Turbine Engines: Operational Experience, Fundamental Mechanisms and Modeling*, Progress in Astronautics and Aeronautics Vol. 210 (American Institute of Aeronautics and Astronautics, Reston, VA, 2005).
[21] Y. Huang and V. Yang, Prog. Energy Combust. Sci. **35**, 293 (2009).
[22] N. Thomas, S. Mondal, S. A. Pawar, and R. I. Sujith, Chaos **28**, 033119 (2018).
[23] N. Rott, Z. Angew. Math. Phys. **20**, 230 (1969).
[24] N. Sugimoto, J. Fluid. Mech. **658**, 89 (2010).
[25] N. Rott, Z. Angew. Math. Phys. **24**, 54 (1973).
[26] N. Sugimoto and M. Yoshida, Phys. Fluids **19**, 074101 (2007).
[27] Y. Ueda and C. Kato, J. Acoust. Soc. Am. **124**, 851 (2008).
[28] M. Guedra and G. Penelet, Acta Acust. Acust. **98**, 232 (2012).
[29] H. Hyodo and N. Sugimoto, J. Fluid. Mech. **741**, 585 (2014).
[30] G. W. Swift, J. Acoust. Soc. Am. **84**, 1145 (1988).
[31] H. Hyodo, K. Muraoka, and T. Biwa, J. Phys. Soc. Jpn. **86**, 104401 (2017).
[32] When the linear perturbation is assumed as $e^{\Lambda t}$, Eq. (21) is called a characteristic equation and the real part of the roots of Λ represents the stability of the system. In this calculation, the imaginary part Ω_I represents the linear stability of the system.